

A Portable Image Overlay Projection Device for Computer-Aided Open Liver Surgery

Kate A. Gavaghan, Matthias Peterhans*, Thiago Oliveira-Santos, and Stefan Weber

Abstract—Image overlay projection is a form of augmented reality that allows surgeons to view underlying anatomical structures directly on the patient surface. It improves intuitiveness of computer-aided surgery by removing the need for sight diversion between the patient and a display screen and has been reported to assist in 3-D understanding of anatomical structures and the identification of target and critical structures. Challenges in the development of image overlay technologies for surgery remain in the projection setup. Calibration, patient registration, view direction, and projection obstruction remain unsolved limitations to image overlay techniques. In this paper, we propose a novel, portable, and handheld-navigated image overlay device based on miniature laser projection technology that allows images of 3-D patient-specific models to be projected directly onto the organ surface intraoperatively without the need for intrusive hardware around the surgical site. The device can be integrated into a navigation system, thereby exploiting existing patient registration and model generation solutions. The position of the device is tracked by the navigation system's position sensor and used to project geometrically correct images from any position within the workspace of the navigation system. The projector was calibrated using modified camera calibration techniques and images for projection are rendered using a virtual camera defined by the projectors extrinsic parameters. Verification of the device's projection accuracy concluded a mean projection error of 1.3 mm. Visibility testing of the projection performed on pig liver tissue found the device suitable for the display of anatomical structures on the organ surface. The feasibility of use within the surgical workflow was assessed during open liver surgery. We show that the device could be quickly and unobtrusively deployed within the sterile environment.

Index Terms—Augmented reality (AR), computer-aided surgery, liver surgery, projection.

I. INTRODUCTION

NUMEROUS studies have demonstrated the benefits of computer guidance for a range of surgical procedures. Navigation systems for the surgery of the head, orthopedics, and, more recently, soft tissue have become commercially available and are an increasingly common addition to the operating room.

Manuscript received December 20, 2010; accepted February 25, 2011. Date of publication March 14, 2011; date of current version May 18, 2011. *Asterisk indicates corresponding author.*

K. A. Gavaghan, T. Oliveira-Santos, and S. Weber are with the Institute of Surgical Technology and Biomechanics, and the ARTORG Centre for Computer Aided Surgery, University of Bern, Bern CH-3012, Switzerland (e-mail: kate.gavaghan@istb.unibe.ch; thiago.oliveira@istb.unibe.ch; stefan.weber@istb.unibe.ch).

*M. Peterhans is with the Institute of Surgical Technology and Biomechanics, and the ARTORG Centre for Computer Aided Surgery, University of Bern, Bern CH-3012, Switzerland (e-mail: Matthias.peterhans@istb.unibe.ch).

Color versions of one or more of the figures in this paper are available online at <http://ieeexplore.ieee.org>.

Digital Object Identifier 10.1109/TBME.2011.2126572

Surgical navigation systems use registered computer-generated 3-D patient-specific models from computed tomography (CT) to display a virtual scene of the surgical procedure, guiding surgeons on a nearby screen. Such virtual reality (VR) systems have proven to assist in the definition and conduct of surgical procedures and in the identification of critical structures. However, the technology requires the surgeon to divert his sight and attention between the virtual information on the screen and the patient. This lack of intuitiveness has called for the development of alternative visual guidance methods and tools. Interest has centered primarily around the development of solutions based on augmented reality (AR).

AR provides a more intuitive view of the surgical navigation data by combining the surgeon's real-world view with virtual 3-D models [1]. The technology allows surgeons to essentially view structures through overlying tissues without the need to mentally align the two scenes. To date, a number of AR technologies have been developed for use in surgery. In video overlay techniques, the superimposition of 3-D computer-generated objects onto real-time images or video, successfully merges the virtual and real-world data. However, complex requirements for camera calibration and registration of video images with the virtual scene have essentially limited the technique to use in surgeries involving relatively fixed workspaces and static anatomical structures such as neurosurgery. Marescaux *et al.* reported the first case of video overlay use in general soft tissue surgery; however, the image merging process was elaborate and time consuming and no accuracy evaluation was provided [2]. In addition, video overlay still requires the surgeon to divide his view between the patient and the AR images displayed on the nearby screen.

In an attempt to remove the need for sight diversion in medical AR technologies, others such as DiGioia *et al.* [3], Blackwell *et al.* [4], Fichtinger *et al.* [5], Masamune *et al.* [6], and Stetten *et al.* [7] later experimented with semitransparent displays that displayed data directly in the view of the patient. Such techniques, termed *image overlay*, allowed surgeons to view the patient and computer-generated 3-D models or 2-D images in a single view. Semitransparent information was displayed in the view of the patient by reflecting computer monitor images off of a semitransparent-silvered mirror placed above the patient. The technology gave the observer an illusion of a 3-D model or 2-D image floating immediately above the patient. Such techniques removed the limitations of video resolution, video quality, and camera field of view but the required setup was obtrusive and workspace was limited to the size of the apparatus. For 2-D image projection of a single plane relative to the angles of the display and mirror, the technique allows data to be viewed from

any perspective; however, 3-D image projection suffers greatly from the effect of parallax and, thus, requires the user to wear a head tracker in order to allow for correction of perspective of the 3-D data.

Fuchs *et al.* [8] and Sauer *et al.* [9] experimented with the use of similar technology in a head-mounted display (HMD). The device removed obtrusive equipment from the surgical scene but like other HMDs, also restricted the surgeon's peripheral vision and motion.

More recently, research has turned to 2-D projection-based image overlay in an attempt to simplify the implementation and reduce the intrusiveness of AR guidance. Sugimoto *et al.* [10], [11] and Tardif *et al.* [12], among others, projected anatomical models onto the patient surface using standard video projectors positioned statically above the patient. Limited by both focal lenses and size, commercially available video projectors cannot be easily moved during surgery. The technique is, therefore, limited to displaying images in a preoperatively defined space at a known distance and angle. Registration in such methods was performed by simply adjusting the position of the patient until landmarks (such as the navel) were visually aligned. However, the absence of accurate and verifiable registration and patient tracking greatly limits the accuracy of the image overlay and does not allow for image correction in case of projector movement.

Despite the current limitations described earlier, the benefits of AR, and in particular projection-based image overlay techniques, are evident. Sugimoto *et al.* concluded that the image overlay assisted in the 3-D understanding of anatomical structures leading to significantly improved surgical outcomes resulting from reductions in operation time, intraoperative injuries, and bleeding [10]. AR was found to aid in the determination of correct dissection planes and the localization of tumors, adjacent organs, and blood vessels [2]. It has been predicted that such technology could be used to avoid injury to invisible structures and to minimize the dissection and resection of neighboring tissues [2].

It can be seen that the projection of anatomical information and surgical guidance data onto the patient is currently the most intuitive AR solution with the largest potential of integration into the routine surgical workflow. The challenges in using this technology lie first in obtaining an accurate registration between the patient and the projected data, and in the calibration of the projection device. Additionally, the technology should fulfill the requirements of being unobtrusive, nonimpeding to the view of the surgeon, and efficient in setup and movement handling. In order to overcome these challenges, we present herein a portable and navigated projection device that is optimized for integration into the surgical workflow.

The proposed image overlay projector device (IOD) uses miniature laser projection technology for portable image overlay. The challenge of patient registration is solved by integrating the projection device into an existing surgical navigation system for liver surgery with a clinically verified registration framework described in [13] and [14].

The calibration of the projection device is calculated relative to a marker shield that can be reproducibly fixed on the IOD

when used in the sterile surgical environment. We, thereby, remove the need for calibration during the intervention and enable the use of standard camera calibration techniques during device development. By using a tracked and lensless laser projector, the projection content can be updated in real time for the current view direction, and focusing on the projection surface is guaranteed. Hence, the IOD can be moved freely in the working volume of the navigation system. The device is small, portable, and minimally intrusive. The projection, which can be performed in close proximity to the organ, remains unobstructed by people or objects and suffers from reduced perspective effects.

In this paper, we present an initial prototype of the image overlay device. We first describe the design, integration and functionality of the IOD in addition to a detailed description of the calibration method. Thereafter, we present verification of the projection accuracy of the device and an initial evaluation of the feasibility of its use in a surgical scenario.

II. METHODS

A. System Overview

The developed IOD incorporates a Microvision development kit (PicoP, Microvision Inc., WA) containing a portable RGB laser projector, a video processor and a microelectromechanical system (MEMS) controller. The projector's MEMS-actuated mirror ($\varnothing_{\text{mirror}}$: 1 mm) reflects the combined RGB laser output, producing an active scan cone of $43.7^\circ \times 24.6^\circ$.

The projector has a resolution of 848×480 pixels, a frame rate of 60 Hz, and light intensity of 10 lm [15].

Unlike conventional projectors, the absence of optical projection lenses and the matching of laser spot size growth rate to the image growth rate result in a projected image that is always in focus. The projector can, thus, be held at any distance from a projection surface providing that sufficient image size and intensity can be maintained.

A protective housing was designed and manufactured using 3-D printing rapid prototyping as depicted in Fig. 1.

The IOD weighs 0.4 kg and is 80 mm \times 80 mm \times 150 mm in size. A hand grip was integrated into the housing design, making the device more ergonomic and preventing slipping when a sterilized sleeve is applied. The device receives DVI/VGA video signal at the base of its handle. A low noise fan for heat dissipation is integrated. An optical reference (comprised of a sterile tracking reference and four passive markers) attached to the outer side of the device housing allows the IOD to be tracked spatially by an optical tracking system. The reference configuration and its placement on the housing were designed to optimize visibility by the position sensor.

B. Usability in the Surgical Environment

The application of a standard transparent sterile drape (Steri-Drape, 3M) that covers the entire IOD and a portion of the attached cable enables the use of the device in a sterile environment. The tracking reference (suitable for autoclaving in standard hospital reprocessing) is attached to the IOD on the outer side of the sterilized sleeve. Passive optical single use marker

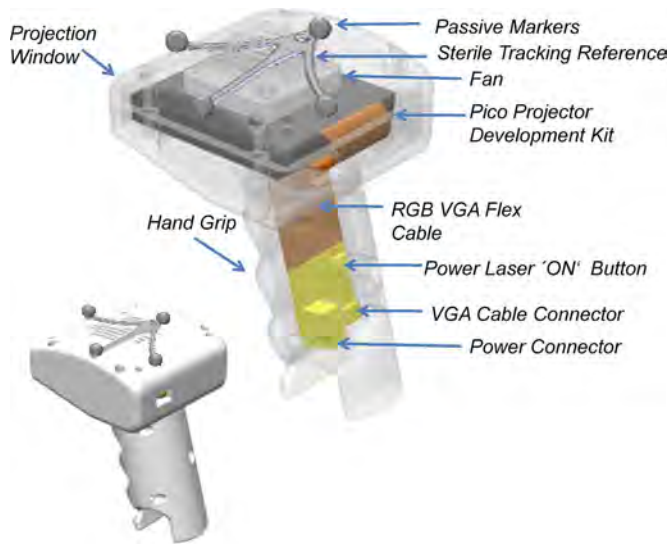


Fig. 1. Design of the handheld image overlay device.



Fig. 2. Liver navigation system used during a liver resection (left) and screenshot of the graphical user interface (right).

spheres (Brainlab AG, Germany) are attached to the tracking reference after sterilization, immediately prior to use.

C. Image Overlay Device Functionality

The IOD can be directly integrated into a surgical navigation system and can, thus, rely on the system's 3-D modeling, calibration, and registration capabilities. As a first application, the IOD was integrated into a liver surgical navigation system developed within our institute (see Fig. 2). The application of the navigation system and its performance in surgery is described in [13] and [14].

A C++ software module, utilizing the QT Development Framework and the Open Inventor libraries, was developed to integrate the IOD into the navigation system.

The module renders images for projection based on tracking and IOD calibration data, in addition to providing a device control interface.

Prior to application of the IOD, the usual tasks required by the navigation application must be completed. Preoperatively, a 3-D surface model consisting of patient-specific structures (typically vessels, liver segments, and tumors) is reconstructed from patient CT using MeVis distant services (MeVis Medical Solutions AG, Bremen, Germany) as described in [16]. During the intervention instruments are calibrated and the VR model is reg-

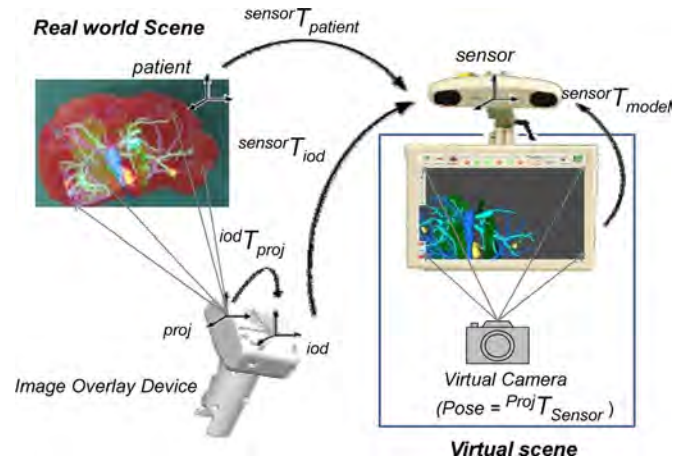


Fig. 3. IOD-integrated system functional model.

istered to the patient using anatomical landmark-based locally rigid registration [13]. Thereafter, the IOD can be activated via the navigation system user interface.

A model of the transformations required for the IOD's functionality is graphically displayed in Fig. 3.

The registration process results in the registration transformation from the patient (*patient*) to the position sensor (*sensor*) ${}^{sensor}T_{patient}$. The 3-D pose of the IOD within the surgical scene is tracked by the navigation system in the coordinate system of the position sensor ${}^{sensor}T_{iod}$. Images for projection are rendered using a virtual Open Inventor camera that captures the 3-D virtual scene of the navigation system.

The virtual camera is defined by the projector's field of view (height angle = 42.6°), and image aspect ratio (1.77) both specified in [15], and the distance to the near and far clipping planes. The pose of the virtual camera is defined as the calibrated projector pose in the sensor coordinate system ${}^{sensor}T_{proj}$ given by

$${}^{sensor}T_{proj} = {}^{sensor}T_{iod} \cdot {}^{iod}T_{proj} \quad (1)$$

where ${}^{iod}T_{proj}$ is the transformation relating the calibrated projection pose to the tracking reference fixed to the IOD.

The rendered images are projected directly onto the liver surface with an update rate equal to the maximum frame rate of the navigation system (20 Hz). If the view of the IOD from the tracking sensor is obstructed, the projection is automatically ceased to prevent the projection of false data.

To effectively project the images onto the target surface in a geometrically correct manner, calibration of the IOD's projection is required. The calibration process is used to define the transformation from the projector to the IOD reference frame ${}^{iod}T_{proj}$. The projector casing was designed to maintain projector position stability even after disassembly and reassembly. Calibration is, therefore, only required during the initial construction of the IOD and after the occurrence of structural changes to the device (e.g., structural damage).

The calibrated transformation ${}^{iod}T_{proj}$ is used to define the pose of the virtual camera and must, therefore, relate the camera model used for the image capture of the virtual scene to the

projector's model of projection. The projection model description and the calibration methodology are presented in the following sections.

D. Projector Calibration Model

For the purpose of projection geometry calibration, projectors are often modeled as reverse pinhole cameras [17], [18]. For ease of coordinate system transformation, the projection transformation that specifies the relationship between the coordinate systems of the projected image and projector is expressed as a projection matrix solution. Using a common calibration camera model [19], the relationship between a point in space and its representation as an image pixel value is given by

$$s\tilde{m} = A[R, T]\tilde{M}. \quad (2)$$

The model relates the 2-D image point $\tilde{m} = [u, v, 1]$ expressed as an augmented matrix to the 3-D real-world point-augmented matrix $\tilde{M} = [X, Y, Z, 1]$ where the extrinsic parameters R and T are the rotation and translation that relate the world coordinate system to the camera coordinate system, s is an arbitrary scale factor, and A is the intrinsic parameters matrix of the camera

$$A = \begin{bmatrix} \alpha & \gamma & u_0 \\ 0 & \beta & v_0 \\ 0 & 0 & 1 \end{bmatrix}. \quad (3)$$

Here, (u_0, v_0) are the pixel coordinates of the principal point; α and β are the scale factors in the axes u and v respectively; and γ is the skew of the two image axes.

The relationship between the parameters and matrices of a virtual object rendered in the virtual scene and the above intrinsic and extrinsic parameters of a real camera are complex. The Open Inventor camera model like other virtual camera models is defined purely by its pose, height angle, and image aspect ratio [20]. The difference in camera models prevents a direct transfer of calibrated projector parameters.

In order to relate the two models, the intrinsic parameters of the Open Inventor camera model were applied to the calculation of the extrinsic parameters $[R, T]$ of the projector.

The Open Inventor virtual camera is modeled as an ideal pinhole camera, and thus, its intrinsic parameters can be easily defined. The scale factors α and β in both axes are said to be equal and the coordinate of the principle point (u_0, v_0) is equal to the center of the image. The camera has no skew between the two image axes ($\gamma = 1$). As neither the virtual camera nor the projector contain optical lens effects, the focal length can be omitted from the extrinsic parameter calculation [21].

The virtual camera provides no method of accounting for distortion and thus, distortion of the projector calculated using Zhang's calibration method, cannot be corrected in the employed image rendering method.

E. Projection Calibration Methodology

Solving the pinhole camera model as described in (1) for the extrinsic camera parameters was achieved through a closed-form solution followed by a nonlinear refinement based on maximum likelihood criterion [19]. The calculation was performed via the

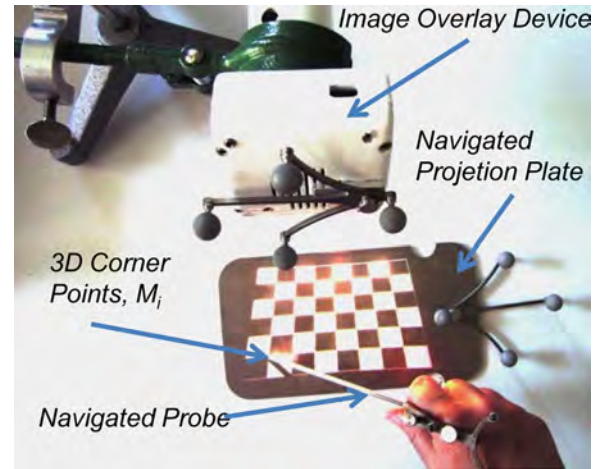


Fig. 4. Acquiring calibration 3-D corner positions with a navigated probe.

Camera Calibration Toolbox for MATLAB [22]. The 3-D real world and 2-D image point pairs $(M, m)_i$ required for the calculation were acquired from a planar pattern, as per Zhang's camera calibration technique [19]. Zhang's technique has been successfully applied in general camera calibration tasks as well as in the calibration of surgical AR systems based on microscopes [23], endoscopes [24], and navigated image viewer systems [25] and was, thus, employed in the calibration of the IOD.

A rectangular grid (8×6 black-white checkerboard pattern, with a resolution of 848×480 pixels) was projected at ten different angles onto a navigated projection plate (*plate*) whose position in space was measured using an optical reference (see Fig. 4).

To obtain sufficient 3-D information from the 2-D projections, projections were performed with the IOD optical axis at angles greater than 45° to the projection plate. The 3-D real-world corner positions M_i of the projected grid patterns were digitized using a navigated pointer in the coordinate system of the plate.

The navigated probe itself was calibrated using the liver navigation system described earlier. The IOD was kept at a distance between 50 and 300 mm from the plane of projection to ensure that the projected images could be easily viewed and did not exceed the size of the plate.

The digitization of each point was performed three times and the positions averaged to reduce the effect of measurement variability. In Fig. 4, the corner digitization setup is depicted.

Corresponding 2-D image pixel coordinates of the checkerboard corners m_i were extracted directly from the image for projection. For each projection, 7×5 point pairs of 2-D pixel values m_i with their respective real-world 3-D projection coordinates M_i were acquired. The overall acquisition process resulted in 350 calibration point pairs.

With the collected point pairs $(M, m)_i$, and the intrinsic camera parameters of the virtual camera A , (1) could be solved for extrinsic parameters $[R, T]$ via the Camera Calibration Toolbox for MATLAB.

The extrinsic parameters $[R, T]$ of each projected image p were calculated and expressed as homogeneous matrices that define the transformations, relating the plate and the calibrated origins

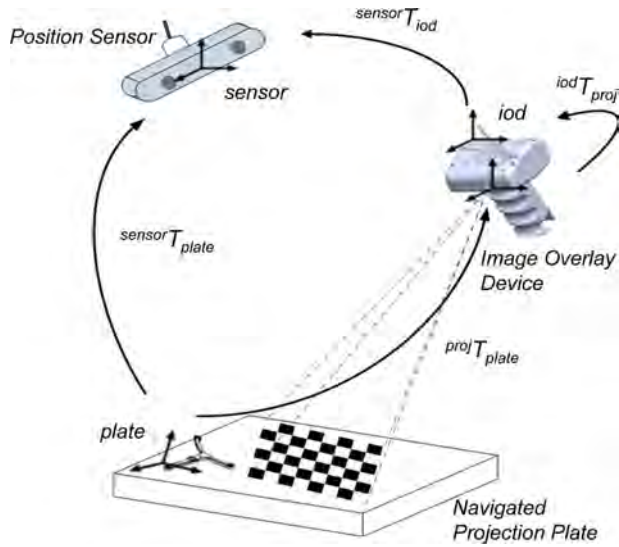


Fig. 5. Image overlay device calibration model.

of projection $({}^{\text{proj}}T_{\text{plate}})_p$ (4).

$$({}^{\text{proj}}T_{\text{plate}})_p = \begin{bmatrix} R_p & T_p \\ 0 & 1 \end{bmatrix}. \quad (4)$$

For each of the ten projections, the transformations from both the navigated projection plate and the IOD to the position sensor $({}^{\text{sensor}}T_{\text{plate}})_p$ and $({}^{\text{sensor}}T_{\text{iod}})_p$, respectively, were recorded and expressed as homogeneous matrices. The transformations relating the calibrated origins of projection to the IOD $({}^{\text{iod}}T_{\text{proj}})_p$ as graphically depicted in Fig. 5 are then given by

$$({}^{\text{iod}}T_{\text{proj}})_p = ({}^{\text{sensor}}T_{\text{iod}})_p^{-1} \cdot ({}^{\text{sensor}}T_{\text{plate}})_p \cdot ({}^{\text{proj}}T_{\text{plate}})_p^{-1}. \quad (5)$$

While the transformation ${}^{\text{iod}}T_{\text{proj}}$ is a static parameter, error introduced during the calibration process results in variance across the set of matrices $({}^{\text{iod}}T_{\text{proj}})_p$.

The transformation with the least reprojection error (as calculated by the Camera calibration Toolbox for MATLAB) was selected to set the pose of the virtual camera and the others discarded.

F. Accuracy Evaluation

Accuracy analysis of the projection was performed on both a planar surface and an irregularly shaped 3-D anatomical surface.

Scenario 1: To test the accuracy of the projector in a closed-loop scenario, the resulting spatial displacement of projecting the aforementioned calibration checkerboard onto a print out of the checkerboard grid was calculated. A planar CAD model of the calibration grid was constructed (Solidworks, Dassault Systems, SolidWorks Corporation, France) and integrated into the virtual scene within the liver navigation system.

A metal plate with checkerboard corner positions marked was registered to a checkerboard virtual model using the conventional landmarks-based rigid registration approach of the navigation system.

The checkerboard was projected as shown in Fig. 6 by means of the IOD software module integrated into the liver naviga-

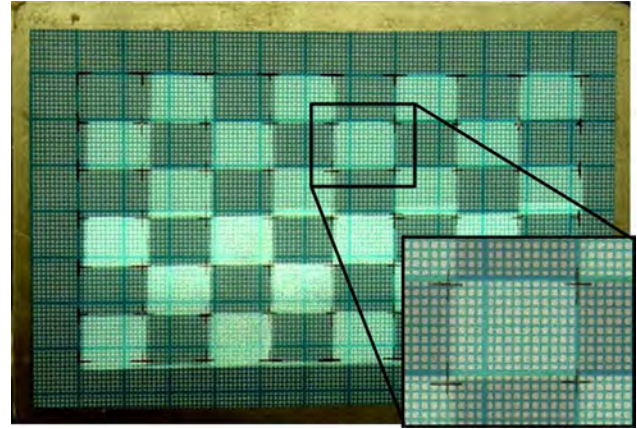


Fig. 6. Projection of the virtual checkerboard onto the checkerboard plate.

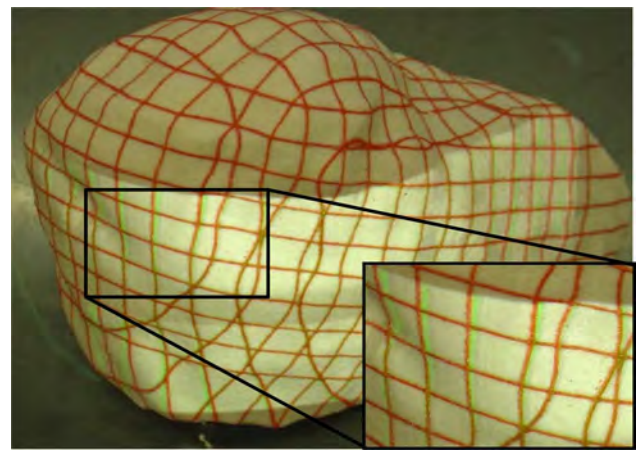


Fig. 7. Projection of the virtual surface grid (green) onto the surface of the liver phantom (grid in red).

tion system. The displacement error of the projection of each checkerboard corner was calculated after digitizing both the grid corner and the projected corner 3-D positions with a navigated pointer tool. Data were collected for three different projection orientations. The first projection (orientation *a*) was conducted approximately normal to the plate while the second and third projections (orientations *b* and *c*) were performed at approximately $\pm 45^\circ$.

Scenario 2: To evaluate the projection accuracy on an anatomically relevant 3-D surface, the aforementioned procedure was repeated with a rigid rapid prototyped model of a human liver with a superimposed 1-cm surface grid (see Fig. 7). The liver model was reconstructed from patient CT data.

G. Clinical Feasibility Evaluation

The feasibility of the IOD for use in computer-aided surgery was evaluated using rigid anatomical models and pig liver tissue in a laboratory setup in addition to a human liver surface during computer-aided open liver surgery.

In the laboratory, patient-specific VR liver models depicting the various anatomical structures, i.e., tumors, resection planes, and blood vessels, were projected directly onto the organ

TABLE I
CALIBRATION UNCERTAINTY

	$R(\omega_x, \omega_y, \omega_z)$ [radians]	$T(X, Y, Z)$ [mm]
E_{max}	(0.05, 0.06, 0.11)	(1.7, 1.4, 7.4)
E_{min}	(0.01, 0.01, 0.02)	(0.4, 0.7, 5.4)
E_{median}	(0.02, 0.03, 0.05)	(1.0, 1.1, 6.1)

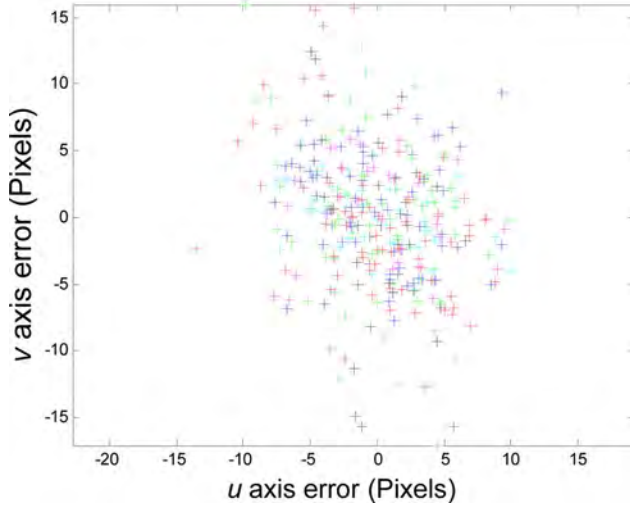


Fig. 8. Reprojection error of each checkerboard corner pair point for each set of calculated calibration extrinsic parameters.

surface. The identification of structures, projection intensity, sterilization procedure, and workspace of the IOD were assessed qualitatively.

In the operating room, the usability of the IOD was evaluated. The IOD was placed in a sterile drape, activated, and operated by the primary surgeon during open liver surgery.

III. RESULTS

The IOD was designed, manufactured, and integrated into the current liver navigation system. Results of the projector calibration and an evaluation of the accuracy of the device projection in addition to feasibility evaluations of the use of the device in clinical scenarios are presented in the following sections.

A. Calibration Results

The uncertainty corresponding to the calibrated extrinsic parameters, expressed as three times the standard deviations of the errors of estimation were calculated by the Camera Calibration Toolbox for MATLAB, and are presented in Table I.

The calculated extrinsic calibration parameters were used to reproject the 3-D point checkerboard corner positions onto the original image. The error in pixels of the reprojected 2-D image corner points to the original image 2-D corner points were calculated for each point by the Camera Calibration Toolbox for MATLAB and are presented in Fig. 8. The errors for each projection (each set of extrinsic parameters) are presented in a different color and demonstrate the effect of the uncertainties presented in Table I.

TABLE II
ANALYSIS OF PROJECTION ERROR

	Scenario 1 Planar projection error [mm]	Scenario 2 3D projection error [mm]
E_{max}	3.59	4.99
E_{min}	0.15	0.17
E_{mean}	1.30	1.32
σ	0.74	0.87

B. Accuracy Evaluation Results

The errors identified when projecting a checkerboard pattern onto a planar surface (Scenario 1) and when projecting a 3-D-shaped pattern of a liver surface onto a 3-D rigid model (Scenario 2) are given in Table II.

The error distribution over the projection surface of both test scenarios for three different projection angles are depicted in Fig. 9.

C. Clinical Feasibility Evaluation Results

The usability of the IOD was first assessed on 3-D rigid liver models and pig liver tissue in a laboratory setup. In ambient light, the projection intensity was perceived to be sufficient to allow structures such as vessels, tumors, and resection planes to be identified.

A projection size of approximately 200 mm \times 350 mm could be obtained before structures become unidentifiable due to decreased light intensity. The intensity of the projector was found to be sufficient to display overlay images that covered a large portion of the human liver. A sample projection, demonstrating projection intensity and color contrast is shown in Fig. 10. The visibility of a range of projected colors on pig liver tissue was qualitatively assessed (see Fig. 11). Colors with greater contrast to the liver tissue (i.e., yellow and green) were identified and used to highlight target structures such as tumors in the projected liver models (see Fig. 12).

While holding the projector still, the effect of normal hand tremor could not be perceived in the projected image. However, due to the latency between position measurement and image projection, image flickering in the projected image is observed when fast purposeful movements are applied to the IOD. Such movements are, however, unnecessary during surgical application and, thus, this effect is not expected to restrict the IOD's use or accuracy.

A sterile drape was applied to the IOD and the projection was found not to be inhibited by its presence. Application of the sterile drape reduced the effectiveness of the device's cooling system but the device still maintained a safe internal temperature for continuous operation times of up to 15 min.

The IOD could be used anywhere in the workspace of the liver navigation tracking sensor as long as the tracking reference remained unobstructed by the device itself (due to holding the device at an excessive angle) or by additional objects.

Finally, the usability of the IOD was evaluated during real liver surgery. Prior to its use, the device was draped and the sterilized optical reference was attached over the drape. The device could be held by the operating surgeon in a single hand or by

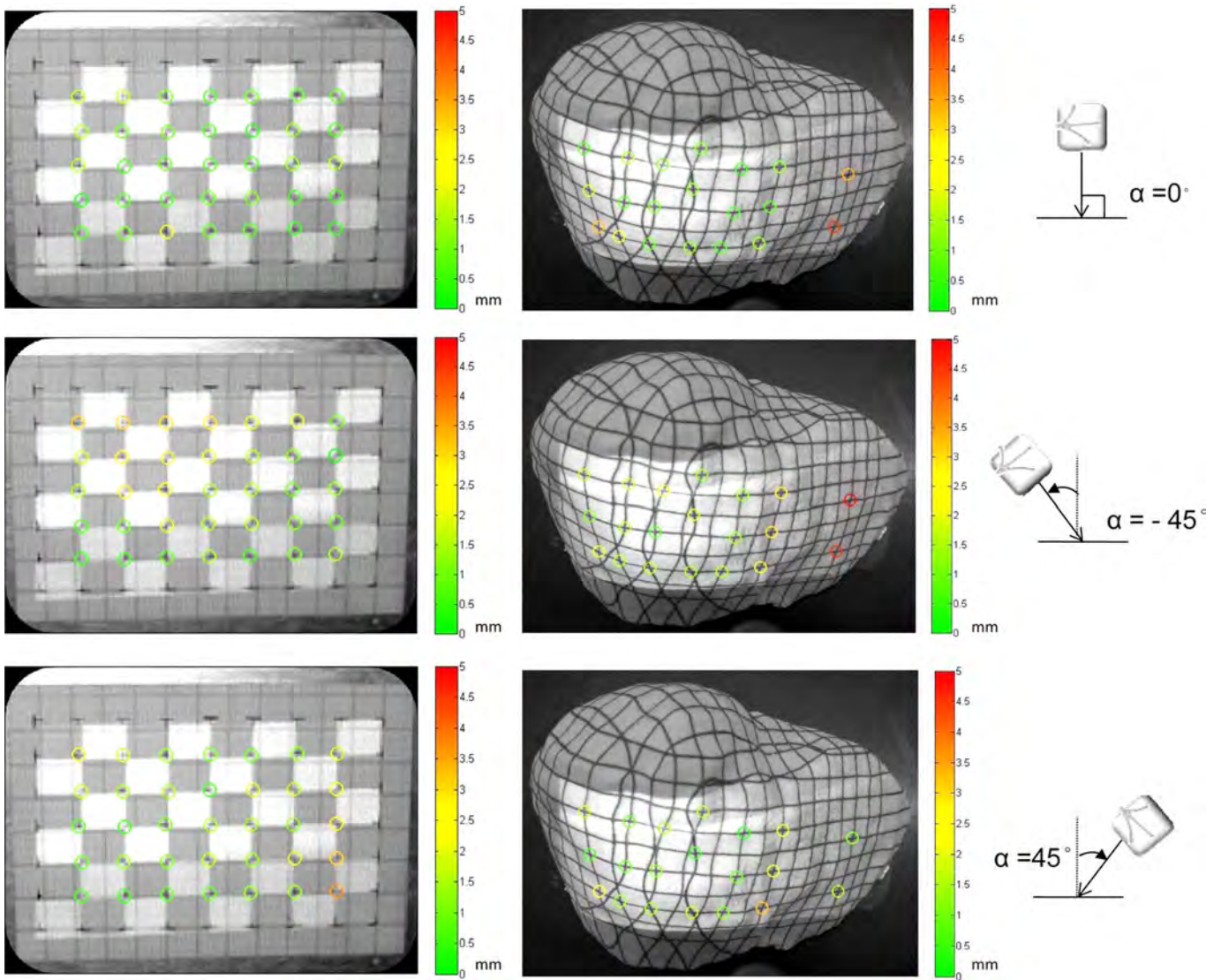


Fig. 9. Accuracy of projected grid lines for a planar checkerboard and 3-D liver model at three different projection angles.

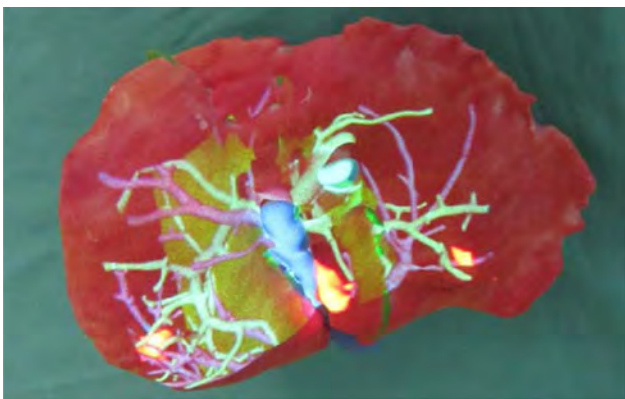


Fig. 10. Projection of 3-D patient-specific liver model images (vessels, tumors and resection planes) on a rigid 3-D printed model of the patient's liver.



Fig. 11. Color visibility comparison projection on pig liver tissue.

an assisting person, allowing the surgeon to perform additional tasks (e.g., cutting, ablation). The device could be quickly and unobtrusively integrated into the surgical environment. After

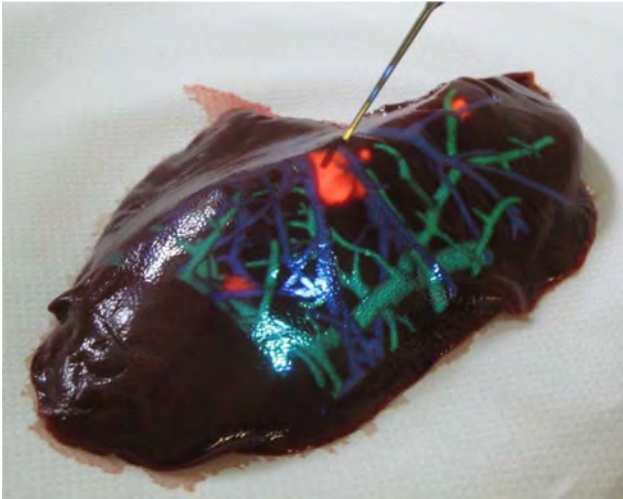


Fig. 12. Projection of liver vessels, tumors, and resection planes on pig liver tissue.

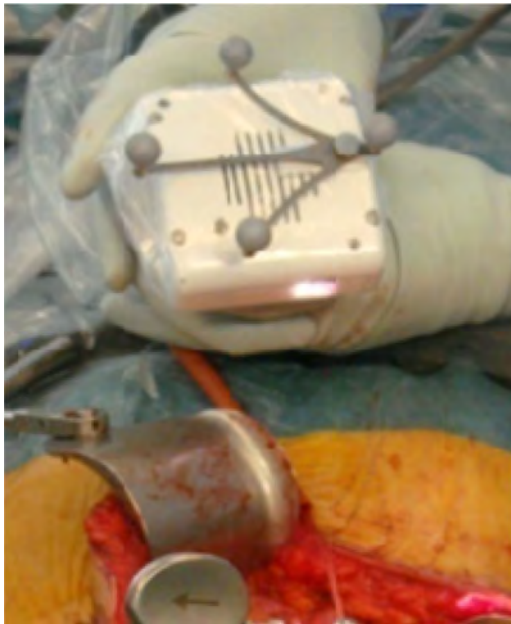


Fig. 13. Application of the projector during a computer-assisted liver resection: holding the projector above the situs.

the surgical overhead lighting had been dimmed, the intensity of the projection was sufficient to allow projected structures to be identifiable on the liver surface. An image from deployment of the IOD in open liver surgery is shown in Fig. 13.

IV. DISCUSSION

The proposed IOD allows for intuitive surgical guidance by projecting target and risk structures directly in the view of the surgeon. By integrating the device into a surgical navigation framework, image overlay is achieved with reduced complexity and virtually no setup time. The use of a handheld projection

device removes workspace limitations caused by permanently installed devices (such as semitransparent mirrors) and avoids line of sight problems that occur with projection devices installed further away from the surgical situs. Moreover, it allows for projections from different view directions.

The accuracy evaluation of the proposed calibration workflow shows that a mean surface projection accuracy of 1.3 mm can be achieved. The resulting projector overlay accuracy is a result of both the calibration process and the (image-to-target) registration accuracy. Through the use of rigid phantoms of known geometry, only a small fraction of the error is expected to originate from the registration process.

The projector calibration method using the inverse of a well-accepted camera model [19] provides consistent results but is limited by the fact that currently no distortion correction was included in the calibration process. The presence of distortion is evident from analysis of the reprojection errors illustrated in Fig. 8. Fig. 9 demonstrates the effect of the projector distortion on the accuracy of the end device, especially at the outer edges of the projected image. The integration of techniques to cope for the inherent distortion of the MEMS-based projection would, therefore, be a primary step to the improvement of the device.

When combining the currently achieved IOD accuracy with our previous experience on the median patient registration accuracy in navigated open liver surgery of 6.3 mm [13], we expect an error of approximately 8 mm for the complete projection system. Such accuracy is sufficient for the current navigation framework. The usefulness of such visualization in a clinical scenario needs to be evaluated in further experiments.

On the technical side, it is evident that further accuracy improvements can be achieved through more accurate patient registration in the navigation framework. For this purpose, an ultrasound-based, nonrigid registration approach is currently being developed.

In addition to the projection inaccuracies, errors originating from the effect of parallax will compromise the resulting surgical accuracy. These effects are kept small in comparison to other techniques due to the close proximity of the projected image to the target structures but are always present when the surgeons view direction cannot be tracked and corrected for. While methods exist to correct for perspective error, the methods can only adjust for a single viewer's perspective and require the use of poorly accepted head worn tracking devices. As the IOD is a portable device, the user can also reduce the effect of parallax by holding the IOD directly in their line of sight.

The usability in the operation room environment was demonstrated through the clinical test in open liver surgery. It could be shown that the proposed sterilization workflow is feasible and causes only a small time overhead during surgery. However, we saw that the effectiveness of the cooling system was compromised by the plastic cover. The device had to be turned off for cooling after approximately 15 min of use. In addition, light intensity was clearly a limiting factor because the available maximal intensity of 10 lm is clearly inferior to the 90 to 160×10^3 lm/m² delivered by state-of-the-art LED-based operating room (OR) illumination. Therefore, the OR lights need to be dimmed while the IOD is being used. This does not present a

significant change in the surgical workflow as dimming of the OR light is also required in other phases of the surgery, for example, when the screen of the ultrasound device or radiological data need to be examined. Furthermore, the achievable light intensity in miniaturized projectors is expected to increase with improvements in laser projection technology.

Although the device was presented as part of a liver navigation system within this study, the technological solution can be used to overlay any registered anatomical model or navigated tool within the workspace of a surgical navigation system. Applications to other surgical problems are currently under investigation. Further, possibilities for increasing system capabilities lie in the integration of other data modalities and image sources into the projection framework. Currently, a 3-D representation of the liver is projected onto the organ. Through the projection process, the 3-D information contained in the data is evidently lost. This depth information could be recovered by coding it into the models being projected as suggested, for example, by Hansen *et al.* [26] or by using 3-D projection technology. Among the additional information that could be integrated into the projection framework, the use of navigated intraoperative imaging such as ultrasound or fluoroscopy could further enhance the anatomical orientation and improve the interpretation of the image data. Moreover, tool guidance information generated by the navigation system (e.g., crosshairs displaying the entry point of a biopsy needle) could be displayed in the projection scenario to enable the execution of image-guided surgery with minimal distraction from the surgical situs.

It is believed that this study is a first step toward the application of the promising miniature projecting technology in medicine and surgery. The technology opens a vast range of application areas and the improvement of the current technological limitations is a subject to research in various groups.

ACKNOWLEDGMENT

The authors would like to thank F. Paci for his contribution to the implementation of the IOD calibration and the design of the IOD housing, M. Oeschger for his contribution to the design of the IOD housing, S. Anderegg for his contribution to the integration of the IOD into the liver navigation system, and the surgeons from the Department of Visceral Surgery and Medicine at University Hospital Bern, Switzerland; Prof. Dr. med. D. Candinas, PD Dr. med. D. Interbitzin, and Dr. med. A. vom Berg for their assistance with intraoperative validation of the device.

REFERENCES

- [1] J. Shuhaiber, "Augmented reality in surgery," *Arch Surg*, vol. 139, pp. 170–174, 2004.
- [2] J. Marescaux, F. Rubino, M. Arenas, D. Mutter, and L. Soler, "Augmented-reality-assisted laparoscopic adrenalectomy," *J. Amer. Med. Assoc.*, vol. 292, pp. 2214–2215, 2004.
- [3] A. DiGioia, B. Colgan, and N. Koerbel, "Computer-aided surgery," in *Cybersurgery: Advanced Technologies for Surgical Practice*, R. Satava, Ed., New York: Wiley, 1998, pp. 121–139.
- [4] M. Blackwell, C. Nikou, A. DiGioia, and T. Kanade, "An image overlay system for medical data visualization," *Lecture Notes in Computer Science, Medical Image Computing and Computer-Assisted Intervention—MICCAI'98*, Cambridge MA: Springer-Verlag, 1998.
- [5] G. Fichtinger, A. Deguet, K. Masamune, E. Balogh, G. Fischer, H. Mathieu, R. Taylor, L. Fayad, and S. Zinreich, "Needle insertion in CT scanner with image overlay—cadaver studies," in *Lecture Notes in Computer Science*, Berlin, Heidelberg: Springer-Verlag, 2004, vol. 3217, pp. 795–803.
- [6] K. Masamune, Y. Masutani, S. Nakajima, I. Sakuma, T. Dohi, H. Iseki, and K. Takakura, "Three-dimensional slice image overlay system with accurate depth perception for surgery," in *Lecture Notes in Computer Science*, London, U.K.: Springer-Verlag, 2000, vol. 1935, pp. 385–402.
- [7] G. Stetten, V. Chib, and R. Tamburo, "Tomographic reflection to merge ultrasound images with direct vision," in *Proc. IEEE Appl. Recog. (AIPR) Annu. Workshop*, 2000, pp. 200–205.
- [8] H. Fuchs, A. State, H. Yang, T. Peck, S. Lee, M. Rosenthal, A. Bulysheva, and C. Burke, "Optimizing a head-tracked stereo display system to guide hepatic tumor ablation," *Studies Health Technol. Informat.*, vol. 132, pp. 126–131, 2008.
- [9] F. Sauer, A. Khamene, B. Bascle, L. Schinunang, F. Wenzel, and S. Vogt, "Augmented reality visualization of ultrasound images: System description, calibration and features," in *Proc. IEEE ACM Int. Symp. Augmented Reality*, 2001, pp. 30–39.
- [10] M. Sugimoto, H. Yasuda, K. Koda, M. Suzuki, M. Yamazaki, T. Tezuka, C. Kosugi, R. Higuchi, Y. Watayo, Y. Yagawa, S. Uemura, H. Tsuchiya, and T. Azuma, "Image overlay navigation by markerless surface registration in gastrointestinal, hepatobiliary and pancreatic surgery," *J. Hepatobiliary Pancreat. Surg.*, vol. 17, no. 5, pp. 629–636, Oct. 2009.
- [11] F. Volonte, P. Bucher, F. Pugin, A. Carecchio, M. Sugimoto, O. Ratib, and P. Morell, "Mixed reality for laparoscopic distal pancreatic resection," *Int. J. Comput. Assisted Radiol. Surg.*, vol. 5, suppl. 1, pp. 122–130, 2010.
- [12] J. Tardif, S. Roy, and J. Meunier, "Projector-based augmented reality in surgery without calibration," *Studies Health Technol. Informat.*, vol. 85, pp. 204–206, 2002.
- [13] M. Peterhans, A. vom Berg, Dagon, D. Inderbitzin, C. Baur, D. Candinas, and S. Weber, "A navigation system for open liver surgery: Design, workflow, and first clinical applications," *IJMRCAS*, 2010, to be published.
- [14] K. J. Oldhafer, G. A. Stavrou, G. Prause, H. O. Peitgen, T. C. Lueth, and S. Weber S, "How to operate a liver tumour you cannot see," *Langenbecks Arch. Surg.*, vol. 394, pp. 489–494, 2009.
- [15] Microvision PicoP Evaluation Kit (PEK) Interface Control Document, no. DC0124473, Rev. C. 2009.
- [16] A. Schenk, S. Zidowitz, H. Bourquain, M. Hindennach, C. Hansen, H. Hahn, and H. Peitgen, "Clinical relevance of model based computer-assisted diagnosis and therapy," *Medical Imaging 2008: Computer-Aided Diagnosis*, vol. 6915, pp. 691502–691519, 2008.
- [17] A. Griesser and L. Van Gool, "Automatic interactive calibration of multi-projector-camera systems," in *Proc. IEEE Comput. Soc. Conf. Comput. Vision Pattern Recog.*, New York, 17–22 Jun. 2006, p. 8.
- [18] M. Kimura, M. Mochimaru, and T. Kanade, "Projector calibration using arbitrary planes and calibrated camera," presented at the IEEE Computer Society Confon Computer Vision and Pattern Recognition, Minneapolis, MN, Jun. 18–23, 2007.
- [19] Z. Zhang, "A flexible new technique for camera calibration," *IEEE Trans. Pattern Anal. Mach. Intell.*, vol. 22, no. 11, pp. 1330–1334, Nov. 2000.
- [20] J. Wernecke, *The Inventor Mentor: Programming Object-Oriented 3D Graphics with Open Inventor*, Release 2, Addison-Wesley, 1994, pp 80–90.
- [21] S. Li, G. Zhang, and Z. Wei, "The determination of the intrinsic and extrinsic parameters of virtual camera based on OpenGL," *6th Int. Symp. Instrum. Control Technol.: Sensors, Automat. Meas., Control, Comput. Simul. SPIE*, vol. 6358 C-1, 2006.
- [22] J.-Y. Bouguet, "Camera calibration toolbox for Matlab[®]," (2010). [Online]. Available: http://www.vision.caltech.edu/bouguetj/calib_doc
- [23] R. Thoranaghatte, J. Garcia, M. Caversaccio, D. Widmer, M. A. Gonzalez Ballester, L. P. Nolte, and G. Zheng, "Landmark-based augmented reality system for paranasal and transnasal endoscopic surgeries," *Int. J. Med. Robot.*, vol. 5, no. 4, pp. 415–422, Dec. 2009.
- [24] J. García, R. Thoranaghatte, G. Marti, G. Zheng, M. Caversaccio, and M. A. González Ballester, "Calibration of a surgical microscope with automated zoom lenses using an active optical tracker," *Int. J. Med. Robot.*, vol. 4, no. 1, pp. 87–93, Mar. 2008.
- [25] S. Weber, M. Klein, A. Hein, T. Krueger, T. C. Lüth, and J. Bier, "The navigated image viewer—evaluation in maxillofacial surgery," in *Lecture Notes in Computer Science*, Berlin, Heidelberg: Springer-Verlag, Oct. 2003, vol. 2878, pp. 762–769.

- [26] C. Hansen, J. Wieferich, F. Ritter, C. Rieder, and H. Peitgen, "Illustrative visualization of 3D planning models for augmented reality in liver surgery," *Int. J. Comput. Assisted Radiol. Surg.*, vol. 5, no. 2, pp. 133–141, Mar. 2010.



Kate A. Gavaghan received the Bachelor degree in computer science from the University of Melbourne, Melbourne, Vic., Australia, in 2003 and the B.S. degree in computer science and B.Eng. degree in electronics and computer systems from the Swinburne University of Technology, Melbourne, Vic., Australia, in 2009. She is currently working toward the Ph.D. degree in biomedical engineering at the Institute for Surgical Technologies and Biomechanics, University of Bern, Bern, Switzerland.

Her research interests include visual and haptic feedback for virtual and augmented reality interfaces for computer-aided surgery and surgical robotics.



Matthias Peterhans received the Ph.D. degree in biomedical engineering from the Institute for Surgical Technologies and Biomechanics, University of Bern, Bern, Switzerland, in 2010.

He currently leads a research group, which develops technology for image-guided soft tissue surgery and is a General Manager of the start-up company CAScination AG, Bern, which provides a surgical navigation system for interventions on the liver. His research interests include medical image processing and computer-assisted surgery.



Thiago Oliveira-Santos received the M.Sc. degree in computer science (computer vision) from the Federal University of Espirito Santo, Vitoria, Espirito Santo, Brazil, in 2006. He is currently working toward the Ph.D. degree in biomedical engineering at the Institute for Surgical Technologies and Biomechanics, University of Bern, Bern, Switzerland.

His research interests include computer-assisted surgery as well as image processing, computer vision and pattern recognition.



Stefan Weber received the degree in electrical engineering and automation from the University of Ilmenau, Ilmenau, Germany.

In 2008, he became an ARTORG Professor for Implantation Technology at the University of Bern, Bern, Switzerland, and since then he directs the ARTORG Center for Computer Assisted Surgery. His research interests include medical device development, particularly for computer-assisted planning and intervention systems, the application of novel technologies in medicine, efficient regulatory affairs, and quality management for fast track clinical evaluation of medical device development.